Design methodology for supersonic ORC turbine blades

Paola Cinnella, Elio, Antonio Bufi

Design methodology for supersonic ORC turbine blades

E.A. BUFI[a,b], P. CINNELLA[b]

a. DMMM, Politecnico di Bari, Bari, Italy (elio-antonio.bufi@ensam.eu)
b. Laboratoire DynFluid, Arts et Métiers ParisTech, Paris, France (paola.cinnella@ensam.eu)

Résumé :

Une méthodologie rapide pour la conception d'aubes de turbines ORC (cycle organique de Rankine) est présentée. Les profils moyens des aubes du stator et du rotor sont générés à l'aide de la méthode des caractéristiques 2D, qui est étendue aux gaz régis par des lois d'état quelconques. Un algorithme permettant de résoudre le problème de l'incidence unique dans le cas de gaz avec un comportement thermodynamique complexe est développé. Les géométries générées par le modèle non visqueux ci-dessus sont ensuite corrigées pour prendre en compte le développement de la couche limite. Les performances des designs sont enfin étudiées à l'aide de simulations numériques basées sur un solveur volumes finis d'ordre élevé disposant de lois d'état et de modèles de propriétés de transport avancés pour les gaz denses.

Abstract :

A fast design methodology for supersonic ORC (Organic Rankine Cycle) stator and rotor turbine blades with low degree of reaction is presented. Both the stator and rotor blade mean-lines are designed by means of the 2D method of characteristics (MOC), extended to gases governed by general equations of state. An algorithm is developed for solving the unique incidence problem in the case of thermodynamically complex gases. Geometries designed according to the preceding inviscid model are then corrected to account for the development of the boundary layer. The final design performances are finally investigated by means of numerical simulations based on a high-order accurate finite volume solver equipped with advanced thermodynamic and transport-property models for dense gases.

Mots clefs/Keywords :

Organic Rankine Cycle, Supersonic Turbine, Method of Characteristics, Dense Gas

1 Introduction

The ORC (Organic Rankine Cycle) technology is used to exploit low-temperature heat sources thanks to the use of low-boiling organic working fluids. The most critical ORC component, along with the heater, is the expander, often a turbine, where the fluid evolves through thermodynamic states close to the saturation curve, characterized by significant dense gas effects.

Furthermore, for compacity and cost reasons, ORC turbines often use a few (one or two) highly loaded stages working in the supersonic/transonic regime. This may concern not only stator but also rotor blades. This can lead to poor turbine efficiency due to the formation of shock waves and shock/boundary layer interactions if the blade passages are not properly designed. The design of supersonic turbine nozzle guiding vane (stator) profiles is traditionally based on the well-known method of characteristics (MOC) [22, 7], an inverse method based on the characteristic form of the compressible Euler equations written for a perfect gas. On the other hand, supersonic rotor blades are most often designed as circular-arc airfoils, although some authors have proposed to use the MOC along with a free-vortex model to design rotor vanes leading to a flow as homentropic as possible across the whole turbine stage [9, 15]. In ORC turbines, the working fluid has a complex thermodynamic behaviour and the perfect-gas model is no longer valid. As a consequence, supersonic blade designs produced under the perfect-gas approximation lead to poor overall performance [10], [21]. In all cases, blade designs also suffer from the development of the viscous boundary layers and, in some cases, local boundary layer separation, which reduces the effective flow section, leading to an effective pressure ratio and reaction degree lower than the nominal ones and to additional losses.

This paper aims to investigate methods for designing supersonic ORC turbine blades that take properly into account dense gas effects. The dynamics of dense gases can be described through the thermodynamic property known as the fundamental derivative of gas dynamics [20] :

$$\Gamma = \frac{a^4}{2v^3}\left(\frac{\partial^2 v}{\partial p^2}\right)_s = 1 + \frac{\rho}{a}\left(\frac{\partial a}{\partial \rho}\right)_s \tag{1}$$

where ρ is the density, $v = 1/\rho$ the specific volume, $a\left[-v^2\left(\frac{\partial p}{\partial v}\right)_s\right]^{1/2}$ the speed of sound, and s the specific entropy. From Eqn. (1) it is seen that Γ represents a measure of the rate of change for the local speed of sound in isentropic transformations. For perfect gases, as well as for light vapours as steam, $\Gamma > 1$ and the speed of sound tends to increase as the fluid undergoes an isentropic compression. For vapours of molecular complex fluids characterized by medium to high molecular weights $\Gamma < 1$ in the saturated vapour region, leading to a reverse behaviour of the speed of sound compared to classical gases. This also affects the behaviour of the characteristic curves. Specifically, Cramer [5] discussed the non-classical behaviour of the Prandtl-Meyer function in the dense gas region, which becomes a decreasing function of the Mach number (rather than increasing) in regions where $\Gamma < 1$. Furthermore, losses associated to the formation of shock waves, described by the relation :

$$\Delta s = -\frac{c^2\Gamma}{v^3}\frac{(\Delta v)^3}{6T} + O((\Delta v)^4) \tag{2}$$

in the weak shock limit, tend to be reduced for shocks with upstream conditions in the dense gas region such that $\Gamma \approx 0$, unlike standard gases for which $\Gamma = O(1)$. In this work, a comprehensive semi-analytical design methodology for 2D stator and rotor ORC blade profiles is proposed. Specifically, we focus on axial turbines although the methodology may be extended to radial ones. For this purpose, following the work of [22], we first extend the MOC to real gases governed by an arbitrary equation of state. Specifically, our MOC is coupled with the advanced

thermodynamic library REFPROP of NIST [11].

In the past Aldo and Argrow [1] developed a MOC for planar and axisymmetric flows of a van der Waals gas into minimum length nozzles. Using a straight sonic line assumption, a centered expansion was used to generate an inviscid wall contour. More recently, Guardone et al. [10] implemented a MOC coupled with the state-of-the-art thermodynamic models to assess the influence of the molecular complexity of the working fluid on the design of supersonic nozzles. Wheeler and Ong [21] extended the MOC to real gases by using and equivalent specific heat ratio thermodynamic model, and used it to design the supersonic part of radial ORC turbine guiding vanes.

In this paper, a MOC generalised to dense gases (DGMOC) modelled by state-of-the-art equations of state is used, for the first time to the authors' best knowledge, for the design of axial supersonic nozzle guide vanes. Subsequently, the DGMOC is coupled to a free vortex model and used for the design supersonic of rotor blade vanes. Rotor design is completed by solving the unique incidence problem for dense gases by means of an iterative algorithm. Finally, boundary layer corrections of the blade geometries are developed, based on an extension of the compressible boundary layer equations to dense gases.
In the following of the paper, we first recall the governing equations and thermodynamic models. Then, we present the DGMOC and the proposed procedures for stator and rotor blade design. Finally, we assess the performance of the resulting blade geometries by means of numerical simulations based on a high-order finite volume solver equipped with advanced thermodynamic and transport property models. The results show that the proposed semi-analytical methodology significantly improves the turbine performance over designs based on standard approaches.

2 Governing equations and thermodynamic models

Dense gases are governed by the conservation equations for single-phase, viscous, non reacting compressible flows, whose conservative form is :

$$\frac{\partial w}{\partial t} + \nabla \cdot (\mathbf{f} - \mathbf{f_v}) = 0 \tag{3}$$

where, $\mathbf{w} = (\rho, \rho\mathbf{v}, \rho E)^{\mathbf{T}}$ is the conservative variable vector, $\mathbf{f} = (\rho\mathbf{v}, -p\mathbf{I} + \rho\mathbf{v}\mathbf{v}, \rho\mathbf{v}H)^{\mathbf{T}}$ and $\mathbf{f_v}$ the inviscid flux, and $\mathbf{f_v} = (0, \tau, \tau \cdot \mathbf{v} - \mathbf{q})^{\mathbf{T}}$ is the viscous flux. In the above equations, $\mathbf{v}$ is the velocity vector, p the pressure, E the specific total energy, $H = E + p/\rho$ the specific total enthalpy, $\mathbf{I}$ the unit tensor, $\tau = 2\mu\left(\nabla\mathbf{v} + \nabla\mathbf{v}^{\mathbf{T}}\right) - \frac{2}{3}\mu\left(\nabla \cdot \mathbf{v}\right)\mathbf{I}$ the viscous stress tensor for a Newtonian fluid, and $\mathbf{q} = -\kappa\nabla T$ the heat flux vector, with κ the thermal conductivity and μ the dynamic viscosity. If $\mathbf{f_v} = 0$, the compressible Euler equations are obtained.

Eqn. (3) has to be supplemented by thermal equation of state (EOS) :

$$p = p(\rho(\mathbf{w}), T(\mathbf{w})) \tag{4}$$

where T is the absolute temperature, and by a caloric EOS related to (4) by the compatibility relation

$$e = e\left(\rho(\mathbf{w}), T(\mathbf{w})\right) = e_r + \int_{T_r}^{T} c_{v,\infty}(T')\, dT' - \int_{\rho_r}^{\rho} \left[T\left(\frac{\partial p}{\partial T}\right)_{\rho} - p\right] \frac{d\rho'}{\rho'^2}$$

TABLE 1 – Thermophysical properties for R245fa, based on reference EOS (from REFPROP ver. 9.1) : critical pressure, temperature and density (p_c, T_c, ρ_c), molecular weight (M_w), acentric factor (ω) and ideal specific heat ratio (γ_{id}), calculated in the dilute gas region along the critical isotherm.

$p_c[MPa]$	$T_c[K]$	$\rho_c[kg/m^3]$	$M_w[g/mol]$	ω	γ_{id}
3.651	427.16	516.08	134.05	0.378	1.061

where e is the specific internal energy, $c_{v,\infty}$ is the ideal gas specific heat at constant volume, quantities with a prime superscript are auxiliary integration variables, and subscript r indicates a reference state. The caloric equation of state is completely determined once a variation law for $c_{v,\infty}$ has been specified.

For viscous flow, Eqn. (3) has also to be supplemented with laws describing the dependency of the dynamic viscosity μ and the thermal conductivity κ on temperature and pressure. Contrary to perfect gases, the dependency on p is generally not negligible for dense gases at temperatures and pressures of the general order of magnitude of the liquid/vapour critical point.

In thermodynamic conditions close to the saturation curve or of the same order of the critical parameters, the validity of the ideal gas equation, which is suitable for low-density states, does not hold anymore. In this work, we consider several dense-gas EOS, and specifically the Peng-Robinson equation with the Stryjek-Vera (PRSV) correction [19] as well as fluid-specific advanced multi-parameter equations available through the NIST-REFPROP library ver. 9.1 [11], referred-to hereafter as the REF models. The DGMOC presented in the following section is coupled with the REF libraries, representing the most accurate available thermodynamic models for a large variety of substances. On the other hand, the numerical simulations presented in section 3 are based on the PRSV, which is much faster in terms of computational time while ensuring a satisfactory accuracy.

In the numerical examples, the working fluid is a well-known organic fluid for ORC applications, the R245fa (pentafluoropropane), which is a hydrofluorocarbon used primarily for closed-cell spray foam insulation (see [17] for application to a multistage transcritical ORC axial turbines). It has no ozone depletion potential and it is nearly non-toxic. Its main thermophysical properties are listed in Tab. 1. For the R245fa, the short technical multiparameter EOS proposed by Lemmon and Span [12] is used, available through the NIST-REFPROP libraries.

3 Design methodology

3.1 Dense-gas method of characteristics (DGMOC)

The MOC is classically employed for the design of the divergent part of supersonic nozzles under the hypotheses of 2D, steady and homentropic flow [22, 7]. Such a flow is governed by the 2D isentropic Euler equations, which represent an hyperbolic system of conservation laws characterized by two families of characteristic lines. These are described by the equations :

$$\frac{dy}{dx} = \tan(\varphi \pm \alpha) \tag{5}$$

where φ is the local flow angle and $\alpha = arcsin(M^{-1})$ is the Mach angle (see Fig. 1). Rewriting the governing equations in the characteristic reference frame leads to the so-called compatibility equations :

$$d\varphi \pm \sqrt{M^2 - 1}\frac{dV}{V} = 0 \tag{6}$$

where $V = |\mathbf{v}|$ is the velocity magnitude, $M = V/a$ is the Mach number, and the sign + or − denotes a left-running or a right-running characteristic, respectively. For a perfect gas, Eqn. (6) can be integrated analytically after rewriting dV/V in terms of M and using the equation of state, leading to the well-known Prandtl-Meyer relation [7] :

$$\varphi \pm \nu(M, \gamma) = \text{constant (along a characteristic line)} \tag{7}$$

where $\nu(M, \gamma) = \frac{1}{\lambda}\tan^{-1}(\lambda\beta) - \tan^{-1}\beta$ is the classical Prandtl-Meyer function, strictly increasing with the Mach number, $\lambda = \sqrt{\frac{\gamma-1}{\gamma+1}}$ and $\beta = \sqrt{M^2 - 1}$. The previous equations, along with the characteristic line equations (5), are then used to design the nozzle wall contour. Typical

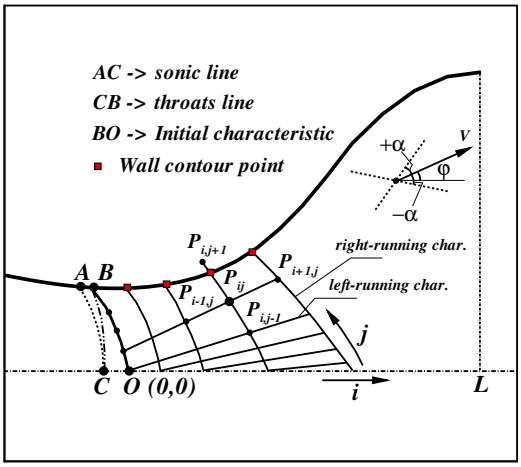

FIGURE 1 – Typical characteristic line patterns and nozzle divergent shape design.

patterns of characteristic lines in the supersonic part of an adapted nozzle is depicted in Fig. 1.

The design procedure for the perfect gas case is described in detail in, e.g., [7]. In the dense gas gase, the classical procedure is modified to account for dense gas effects. The main consequence of considering dense gas EOS is that the characteristic equations (5), (6) can no longer be integrated analytically and the characteristic lines must be calculated through a numerical procedure [22]. Like the classical MOC, the DGMOC approach, described hereafter, is constituted of an initialization and a iteration step.

The algorithm takes as inputs the target mass flow rate G (kg/s), the upstream total pressure p_0 (Pa) and temperature T_0 (K), and a target pressure (or Mach number) distribution along the nozzle axis $p(x)/p_0$. The latter is chosen in such a way to reach the desired exit conditions without discontinuities or too rapid accelerations, which could cause disturbances or shock waves.

In the initialization step, the first characteristic ξ_0 originating from point B in the throat region (see Fig. 1 is reconstructed as a piecewise line by using a potential flow solution for perfect

gases (Carriere's method, see [7]), and an equivalent specific heat ratio γ_{eq} approximation. In our calculations, the characteristic ξ_0 is discretized by 50 points. Given the initial data (p_0, T_0), $p(x)/p_0$ and G, and assuming a chock conditions in the nozzle throat, the sonic conditions are then evaluated. Afterwards, the nozzle axis is discretized by using uniformly spaced points (typically 100 points are used). The dense gas EOS are used to compute the static enthalpy along the axis $h(x) = h(p(x), s)$ and the velocity magnitude $V = \sqrt{2(h_0 - h)}$, where $s = s(p_0, T_0)$ and $h_0 = h(p_0, T_0)$ are constant throughout for a homentropic flow. All of the preceding flow properties are evaluated as function of normalized geometrical coordinates and renormalized in the physical plane.

With the initialization completed, the MOC procedure is applied iteratively to march the solution from the nozzle throat to the exit. The compatibility equation along a characteristic line ξ_i (6) is discretized at each point P_{ij} in the supersonic nozzle flow (see Fig. 1) by using finite differences :

$$\overline{A}(V_{ij} - V_{i,j-1}) \pm (\varphi_{ij} - \varphi_{i,j-1}) = 0 \tag{8}$$

where $\overline{A} = (A_{ij} - A_{i,j-1})/2$, with $A = \sqrt{M^2 - 1}/V$. This is integrated numerically along with (5) by using the Heun method, which ensures second-order accuracy (see [22]). The dependent variables (V_{ij}, φ_{ij}) and the coordinates (x_{ij}, y_{ij}) are then obtained.
The integration along a characteristic is stopped when a criterion based on the target massflow is satisfied.

The DGMOC has been implemented in a FORTRAN code named NODEC (NOzzle DEsign with method of Characteristics). Although the iterative integration procedure of the compatibility equation required for the advanced EOS is more complex than the analytical expression available for the perfect gas model, the algorithm remains very fast, and only few seconds are required for obtaining accurate nozzle shapes on a single-processor machine.

3.2 Nozzle guide vane design

The nozzle geometry generated by the MOC is geometrically post-processed to obtain the supersonic guide vane of an axial ORC turbine. The guide vanes are designed as a two dimensional linear cascade. Given the main turbine geometrical characteristics, and namely the axial chord ch, the exit flow angle θ_f, and the blade pitch l_{pitch}, the blade vane is designed in the following way (see Fig. 2) : the suction side (d-e) is obtained by rotating the MOC nozzle geometry by the angle θ_f in clockwise direction. Then, given ch and the coordinates of point (c), the leading edge (d-b) is designed as a circular arc with radius R_1. The latter is chosen such that $R_1/2h_t > 6$, as proposed in [7], to avoid excessively high flow deflections which could induce separation. The pressure side part of leading edge (c-b) is designed as a circular arc of radius R_2, whose angular extension ϕ_r is a free parameter. The pressure side (b-a) is designed as a third order polynomial verifying the constraints given by the end-points coordinates (a)-(b) and the angles ϕ and Θ. The aft part (a-f) is determined by translating and cutting the nozzle profile by a distance equal to the pitch l_{pitch}. Finally, a third order polynomial fits the points (f)-(e) in order to obtain the trailing edge.

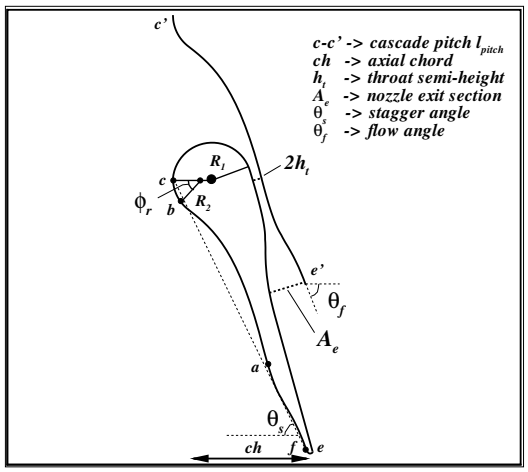

FIGURE 2 – Sketch of the geometrical post-processing used for the design of the axial ORC nozzle guide vane profile.

3.3 Supersonic rotor blade design

In this section, we extend the design procedure initially proposed by Goldman [**?**] and Paniagua [**?**] to the design of supersonic rotor blades under a dense gas model. First of all, we assume that the supersonic flow at the rotor inlet is uniform, that it is deflected by the rotor blades and returns to uniform conditions downstream of the rotor. To achieve this deflection smoothly, the flow passes through a transition region delimited by upper and lower transition arcs and by characteristic lines. For clarity, the transition region is sketched in figure 3, where the

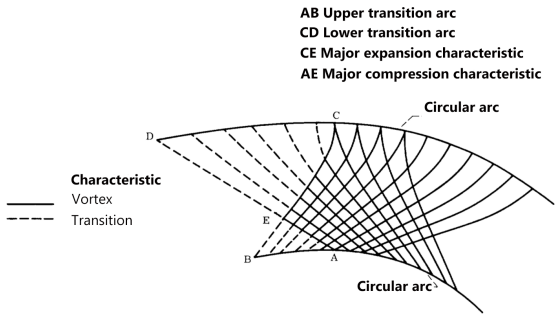

FIGURE 3 – Scheme of the system of characteristic lines in the rotor vane. Extracted from [**?**].

blade portions AB and CD are referred-to as transition arcs, and the dashed lines are used to represent the characteristics. Through this region, the uniform flow is converted into a free vortex flow and *viceversa* following an isentropic transformation.
Figure 4 provides a schematic description of the rotor blade geometry designed with MOC.

As an input to the design procedure we consider the following parameters : the inlet relative total pressure and temperature, the inlet and outlet relative flow angles β_i and β_o, the inlet and outlet relative Mach numbers M_i and M_o, the (constant) Mach number M_l prescribed for the lower circular arc b-b', and the (constant) Mach number M_u prescribed for the upper circular arc d-d'. With this data, the procedure calculates the coordinates of the lower and upper transition arcs (a-b/a'-b' and d-e/d'-e' for inlet and outlet, respectively), written in the

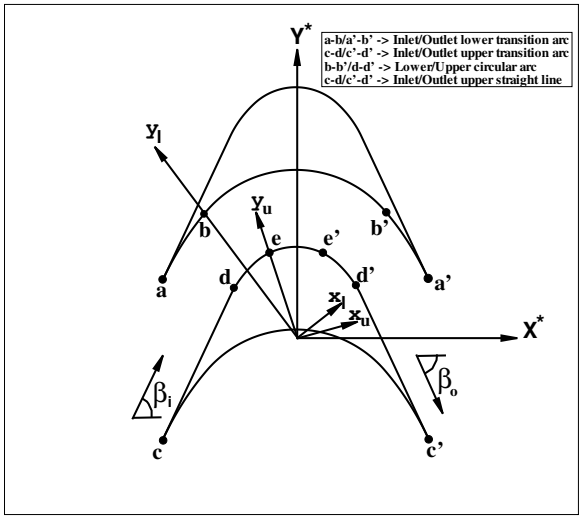

FIGURE 4 – Schematic description of the rotor blade design.

unrotated lower/upper reference systems (denoted with subscripts l and u). The upper and lower transition arcs are designed by marching from the vortex region to the uniform region, in order to match the input inlet/outlet conditions.
The vortex flow is described by the equation $V \cdot R = \text{cost}$, with V the velocity magnitude and R the curvature radius of the relative streamline. This can be re-written in non-dimensional form by normalizing with respect to the product $a^* \cdot r^* = \text{cost}$, where the super-script $*$ denotes critical (sonic) parameters. Specifically, a^* represents the critical speed of sound and r^* the radius of the sonic streamline. The vortex equation becomes : $M^* \cdot R^* = 1$, with $M^* = V/a^*$ and $R^* = R/r^*$.

The vortex flow is then used as the initial condition for the characteristic equations, used to determine the transition arcs. These are designed in a marching manner by adding straight wall segments that produce a small change $\Delta\varphi$ in the flow angle and the respective variation in the Mach number. While for a perfect gas this can be done by using analytical expressions for the Prandtl-Meyer function $\nu = \nu(M)$ and the critical Mach number $M^* = M^*(M)$, for generic dense gas EOC an iterative numerical procedure is developed (not reported for brevity). Similarly, an iterative procedure is developed to calculate M given M^*. Once M_l^* has been determined from M_l, by using the iterative procedure, the algorithm described in [15] is applied to calculate the geometry of the lower transition arc.

The definition of the rotor geometry is then completed with the straight line parts c-d/c'-d' and the circular arcs b-b'/d-d' (see Fig. 4). Finally, a finite leading-edge/trailing-edge thickness is added. Note that blades with various degrees of reaction can be designed by prescribing suitable values for the outlet parameters.

The rotor design procedure has been implemented in a FORTRAN code named RODEC (ROtor DEsign with method of Characteristics). The RODEC algorithm has been run for different fluids and design conditions to investigate the impact of real gas effects on the resulting geometry. The degree of reaction is set to zero so that the resulting blade is always symmetric. Figs. 5a-b show a comparison of geometries calculated for R245fa (see Tab. 1 for properties) with different operating conditions and gas models. The operating conditions considered for the design, are

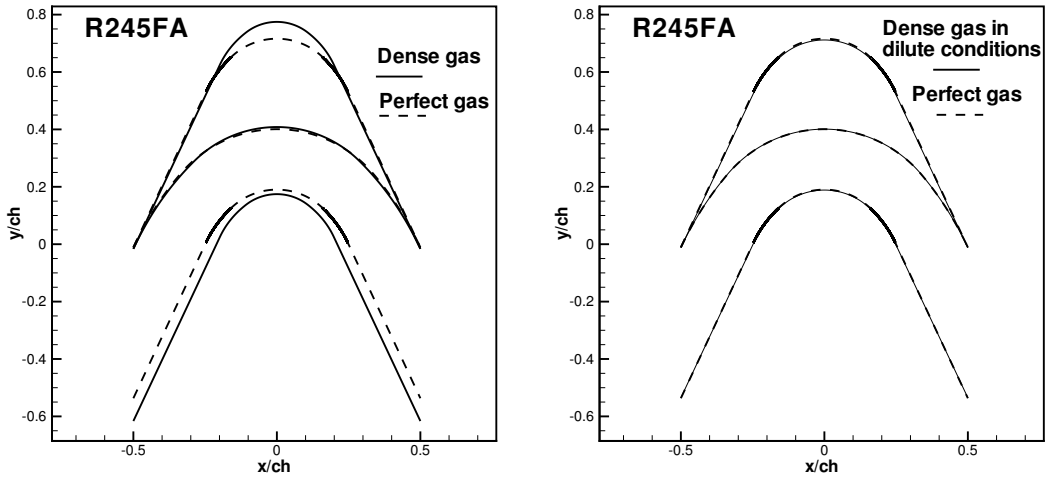

(a) (b)

FIGURE 5 – Blade designs for R245FA at operating conditions ($p_r^0 = 1.05, T_r^0 = 1.05, M_{in} = M_{out} = 1.5$) (a) and at dilute conditions ($p_r^0 = 0.055, T_r^0 = 1.15, M_{in} = M_{out} = 1.5$)(b). Dashed lines represent designs obtained under the perfect gas model.

TABLE 2 – Operating and design conditions for the rotor design.

p_r^0	T_r^0	M_{in}	M_{out}	M_l	M_u	β_{in}	β_{out}
1.05	1.05	1.5	1.5	1.0	2.0	65°	65°

given in Tab. 2. The first operation point is very close to the R245fa upper saturation curve and this affects the rotor geometry leading to larger cross section variations with respect to perfect gas. Specifically, the dense gas design is characterized by a greater exit-to-throat area ratio. In figure 5b the test is repeated by lowering the total pressure and increasing the total temperature in order to reach the dilute dense gas region. In this region, the blade designed with a dense gas EOS is very similar to that obtained with the perfect gas model. Indeed, the two blade geometries are practically overlapped. Then, a parametric study for several working fluids suitable for ORC applications at the same reduced input conditions has been carried out. In Tab. 3 the following output geometrical parameters are given : the blade solidity σ, defined as the axial chord to pitch ratio, the axial chord ch^*, and the pitch ph^* normalized respect to the critical radius r^*. It can be noticed that the lower is the fluid molecular complexity, which is inversely related to the specific heat ratio in the dilute gas limit γ_{id}, the higher is the solidity.

3.4 Calculation of the unique incidence for dense gases

The presence of a finite leading edge thickness for the rotor blades, induces the presence of a bow-shock due to the supersonic incident relative flow. Assuming the rotor to be in a started condition (i.e. the relative flow is fully supersonic in the blade vane), some cautions have to be taken into account due to peculiar aerodynamic phenomena involved.

From perfect-gas aerodynamics of supersonic blade cascades, it is known that in a started turbine the relative inlet flow angle is not always a free parameter, but for some flow configurations it is a function of the inlet Mach number [2]. This behaviour has consequences on

TABLE 3 – Rotor geometrical output parameters for four different organic fluids under the same operating condition ($p_r^0 = 1.05, T_r^0 = 1.05$, $M_{in} = M_{out} = 1.5$, $M_l = 1$, $M_u = 2$,$\beta_{in} = \beta_{out} = 65°$), and thermophysical properties of the fluids in terms of molar mass $M_w[\frac{g}{mol}]$ and ideal specific heat ratio γ_{id}.

	R245fa	**Novec649**	**RE347mcc**	**R449**
σ	1.67	1.59	1.62	1.60
ch^*	2.45	2.50	2.50	2.53
ph^*	1.47	1.56	1.54	1.58
M_w	134.05	316.04	200.05	250.00
γ	1.061	1.027	1.039	1.030

the definition of the inlet boundary condition and is known as the *unique incidence* problem. By considering the pattern of characteristic lines departing from the leading edge of a rotor

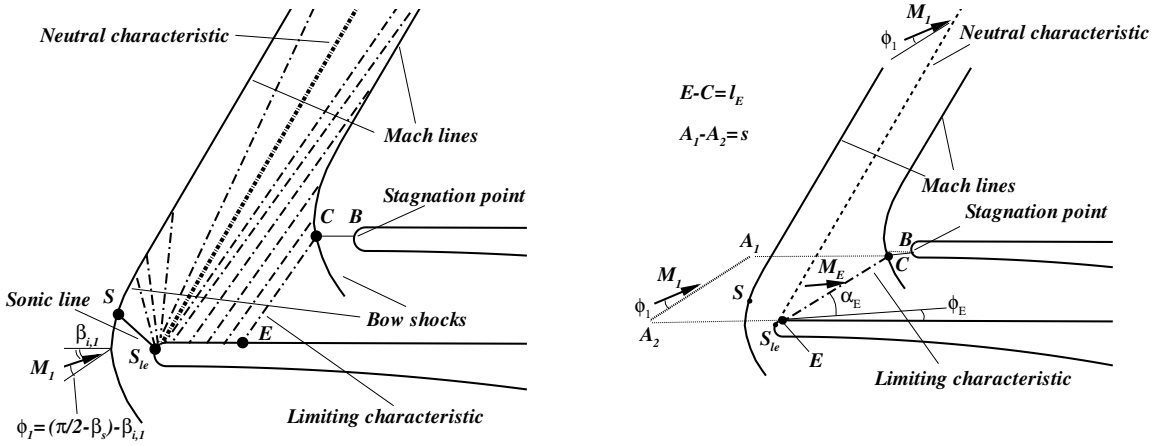

(a) (b)

FIGURE 6 – Characteristics pattern and expansion fan lines for a supersonic rotor (a) ; definition of the control volume upstream and downstream of the bow-shock (b).

with an incident supersonic and axial subsonic flow (see Fig. 6a), the analysis is carried out by making the hypotheses of *simple wave* characteristic lines, which means that all the characteristics are considered as straight lines. Besides, the bow-shocks are considered to become Mach lines far from the leading edges and only the influence of the first adjacent shock leg is taken into account. In this framework, the supersonic flow is slightly decelerated by the bow-shock, then the deflection imposed by the suction side part of the rounded leading edge leads the flow to expands by means of an expansion fan. The flow, which is subsonic in region close to the leading edge, accelerates again to supersonic conditions after crossing the sonic line $S - S_{le}$. Then, it further accelerates on the suction side through a supersonic expansion fan and reaches the Mach number defined by the *limiting characteristic* emanating from point E. The latter, known also as the *last captured Mach wave*, connects the intersecting point between the detached shock wave C and the stagnation streamline with point E on the suction surface of the adjacent blade. Besides, it sets the limit for the maximum massflow allowable for the

given flow configuration. Inside the pattern of characteristic lines it can be shown that only one exists (the "unique") which does not intersect the bow-shocks. This characteristic has the property to meet the far field without disturbances and all the properties of the homogeneous supersonic inlet flow are conserved along this line, called *neutral characteristic*. By considering this feature, the functional dependency of the *unknown* inlet flow angle from the inlet Mach number M_1 can be deduced from the mass conservation across the bow-shock. The control volume, as proposed by Starken [18], is chosen as limited far upstream the shock wave by a straight surface of extension equal to the cascade pitch $s = A_1 - A_2$, and downstream by the limiting characteristic of length $l_E = E - C$, see Fig. 6b. Depending on the Mach number M_1, the limiting characteristic point E on the adjacent suction side could be either on the straight part, where the flow is horizontal in the rotated reference frame with flow angle $\phi_E = 0$ (see Fig. 6a) and on the rounded leading edge , with $\phi_E > 0$ (see Fig. 6b). Besides, the position of the stagnation point C is dependent from the incident flow direction. For the sake of generality, these configurations are taken into account in the following analysis.
By using the notation defined in Figs. 6 (here the flow angle is evaluated as $\phi_1 = (\pi/2 - \beta_s) - \beta_{i,1}$, where β_s is the stagger angle and $\beta_{i,1}$ the incidence angle) and applying the mass conservation on the control volume defined previously, the following equation holds :

$$\rho_1(V_1 \sin\phi_1)s = \rho_E(V_E \sin\alpha_E)l_E \tag{9}$$

In the preceding equation, V_1 and V_E are the velocity magnitudes of the flow at the control volume surfaces, whereas α_E is the Mach angle associated to the limiting characteristic. This equation can provide the unknown inlet flow angle ϕ_1, which is the solution to the unique incidence problem, if all the quantities on the right hand side are calculated in advance. Firstly, the limiting characteristic line length l_E, defined as the distance between the stagnation point on the bow-shock C and the point E, requires the definition of the point C position. This is a function of the bow-shock stand-off distance from the stagnation point on the leading edge B, $B-C$, depending on the intensity of the shock (i.e. on M_1), and on the leading edge radius. In order to estimate it, the procedure proposed by Moeckel is followed [14], with modifications for dense gas effects, which mainly consist in introducing numerical iterations on the EOS wherever no explicit analytical solution is available. Details can be found in [3].

The methodology, also implemented in the RODEC code, converges quickly to a solution which provides the actual inlet relative flow angle, useful to solve the periodicity problem related to the unique incidence of isolated supersonic rotors and the correct definition of the inlet boundary condition.
In Fig. 7 a comparison between the incidence flow angles, $\beta_{i,1}$, calculated with the procedure described above for the R245fa fluid, in dense ($p_r^0 = 0.1$, $T_r^0 = 0.95$) and dilute ($p_r^0 = 0.01$, $T_r^0 = 1.18$) gas conditions, has been carried out for a blade with r/s 0.05 (with r the leading edge radius and s the cascade pitch) and a stagger angle $\beta_s = \pi/3$. It can be noticed that the dense gas solution provides higher values of ϕ_1 for the same M_1. Since $0 < \phi_1 < \beta_s$, being $\phi_1 = 0$ and $\phi_1 = \beta_s$ the limits of the strongest and weakest admissible bow-shock respectively, the dense gas solution provides a less shock-influenced inlet flow angle than the dilute one. This behaviour can be explained by the fact that dense gas effects decrease the strength of the bow-shock.

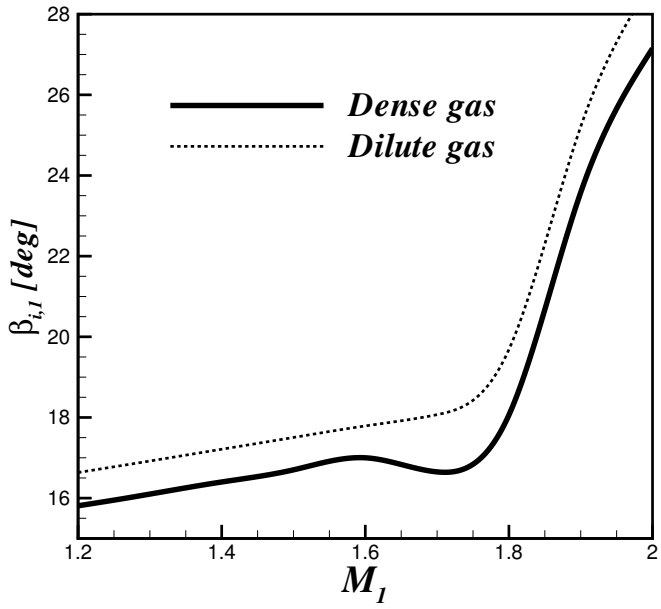

FIGURE 7 – Unique incidence solution and comparison of the incidence flow angle, $\beta_{i,1}$, as function of the inlet Mach number M_1 for the R245fa fluid in dense ($p_r^0 = 0.1$, $T_r^0 = 0.95$) and dilute ($p_r^0 = 0.01$, $T_r^0 = 1.18$) gas conditions. The solution is evaluated for a r/s ratio of 0.05 (with r the leading edge radius and s the cascade pitch) and a stagger angle $\beta_s = \pi/3$.

3.5 Boundary layer corrections

Viscous effect have a considerable influence on the performance of nozzle guide vanes and rotor blades designed by using the inviscid MOC. Specifically, for nozzle guide vanes, viscous losses can reduce the ideal isentropic efficiency by about 10%. Additionally, the boundary layer reduces the effective exit-to-throat area of the nozzle guide vane, leading to an expansion ratio below the target one. For rotor blades, the boundary layer reduces the degree of reaction and increases losses. To palliate these kind of problems, the presence of boundary layer should be taken into account in the preliminary design. The idea is to use the inviscid wall pressure distribution to evaluate the development of the boundary layer thickness and to correct the inviscid design accordingly. In order to take into account these effects in a preliminary design stage, an approximate calculation of the compressible turbulent boundary layer subject to an arbitrary pressure gradient is carried out by following the Reshotko-Tucker method [16], with modifications for real gases. The latter involves the momentum integral and momentum-of-momentum equations as simplified by using the Stewartson-Illingworth's transformation. The Ludwieg-Tillmann skin-friction relation is used in these equations in a form suitable for compressible flows. A power-law is used for the turbulent velocity profile close to the wall, whereas a quadratic Crocco's law is used for the temperature distribution. The equations above are written such that no hypotheses on the equation of state are done.

The method is developed under the assumption of a constant Prandtl number of the order of 1, constant pressure along the direction normal to the wall and flat plane adiabatic surface. In this case it is possible to write the boundary layer integral momentum equation, along with the auxiliary momentum-of-momentum equation in terms of the incompressible form factor H_i, as

follow :

$$\frac{d\Theta_{tr}}{dx} + \frac{\Theta_{tr}}{M_e}\frac{dM_e}{dx}\left[2 + H_i\right] = 0.5 \times C_f \tag{10}$$

$$\begin{aligned}\frac{dH_i}{dx} = &-\frac{1}{M_e}\frac{dM_e}{dx}\left[\frac{H_i\left(H_i+1\right)^2\left(H_i-1\right)}{2}\right] - \\ &- 0.03H_i\left(H_i^2-1\right)0.5 \times \frac{C_f}{\Theta_{tr}}\end{aligned} \tag{11}$$

where Θ_{tr} is a "transformed" momentum thickness by means of the Stewartson-Illingworth transformation [6], M_e is the external Mach number (obtained from the inviscid MOC calculation) and C_f is the skin friction. The coefficient -0.03 in Eqn. (11) results by introducing the Maskell empirical approximation [13] for the shear stress integral term in the original momentum-of-momentum equation :

$$\int_0^1 \frac{\tau}{\tau_w} d\left(\frac{Y}{\Delta}\right) = 1.03\frac{H_i}{H_i+1} \tag{12}$$

where τ is the shear stress, τ_w the wall shear, Y and Δ are the transformed wall distance and boundary layer thickness, respectively. The transformed momentum thickness Θ_{tr} is related to the compressible one as $\Theta = \Theta_{tr}\frac{p_0}{p_e}\frac{a_e}{a_0}$, where p_0 and a_0 are the free stream total pressure and speed of sound, respectively. In order to close the problem, the skin friction coefficient C_f needs to be evaluated. For this purpose, the transformed compressible form of the Ludwieg-Tillmann equation for turbulent boundary-layer is used. Besides, it is written such that all the thermodynamic variables are explicitly calculated by using a generic EOS. By writing the skin friction in terms of transformed variables and applying Eckert's [8] reference enthalpy method the following form is obtained :

$$\begin{aligned}C_f = &\frac{\tau_w}{0.5\rho_{ref}u_e^2} = \\ =&0.246e^{-1.561H_i}\left(\frac{M_e a_0 \Theta_{tr}}{\nu_{ref}}\right)^{-0.268}\left(\frac{\rho_e}{\rho_{ref}}\right)\left(\frac{p_e}{p_0}\right)^{-0.268}\end{aligned} \tag{13}$$

In the above equation the subscript "ref" states a variable calculated at a reference temperature. Here the Eckert method is applied, such that the reference temperature is calculated as $T_{ref} = 0.72T_0 + 0.28T_e$. In this way the variation of viscosity with temperature is taken into account and its value is calculated at the local T_{ref} with the selected EOS. Finally, the velocity and temperature distribution close to the wall are approximated by a power-law and quadratic Crocco's equation, respectively, as $\frac{u}{u_e} = \left(\frac{y}{\delta}\right)^{\frac{1}{7}}$, $T = T_0 + \left(T_e - T_0\right)\left(\frac{u}{u_e}\right)^2$.

Equations (10) and (11) represents a system of coupled first order ordinary differential equations which can be numerically solved by means of fourth order Runge-Kutta method. The method is carried out starting from the throat section of the inviscid nozzle throat and the leading edge of the inviscid rotor blade. In the first case, it is supposed that the boundary layer thickness is not zero (due to the development of the convergent), but reaches an extremum. This corresponds to imposing the initial condition $\frac{d\Theta_{tr}}{dx}_{throat} = 0$. From (10) the initial value for Θ_{tr} is then evaluated. For the rotor, the boundary condition $\Theta_{tr}(x = 0) = 0$ is imposed. For both rotor and nozzle the initial value $H_i = 1.1$ is selected. Indeed, as explained in [16], for blunt bodies a good initial guess value for the form factor is between 1.0 and 1.3. The error committed in this

choice is inconsequential, since the form factor will tend to reach its proper value in the first few steps of calculation. The integration of equations (10)-(11) leads to the $\Theta_{tr}(x)$ distribution along the nozzle/rotor blade wall. The effect of the wall curvature is neglected.

The compressible momentum thickness Θ is calculated by means of its functional relation with the transformed variable, then the boundary layer thickness δ is calculated in order to satisfy the definition $\Theta = \int_0^\delta \frac{\rho u}{\rho_e u_e}\left(1 - \frac{u}{u_e}\right) dy$. The displacement thickness is evaluated as $\delta^* = \int_0^\delta \left(1 - \frac{\rho u}{\rho_e u_e}\right) dy$. The above integrals are numerically solved with a 16 point Gauss-Legendre quadrature method.

Finally, the inviscid shape $S(x)_{inviscid}$ calculated with the MOC is corrected as $[S(x)_{inviscid}+\delta^*]$. In order to ensure convergence of the numerical methodology, the inviscid shape is used as base for an interpolated curve passing from a high number of points equally spaced. In Fig. 8 and Fig. 9 the boundary layer correction is applied at the inviscid nozzle guide vane and rotor shape, respectively. By comparing the blade shapes with and without the correction, it can be noticed an increase of the nozzle exit-to-throat area ratio and a non-symmetric shape for the rotor, which implies a recover of the degree of reaction.

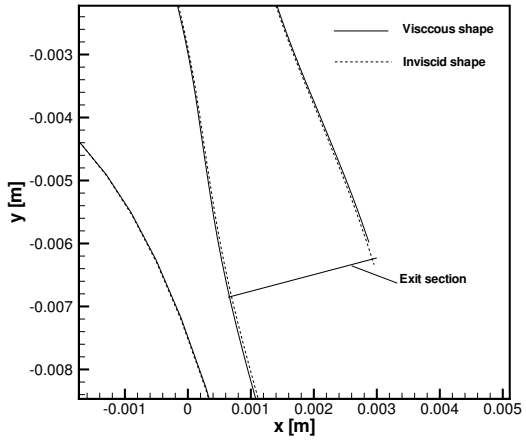

FIGURE 8 – Comparison between inviscid and viscous nozzle guide vane shapes with view enlargement of the exit section.

4 Numerical assessment of the designs

The preceding design methodology for nozzle guide vanes and rotors has been verified by means of numerical simulations. For this purpose, a dense gas solver based on a third-order accurate finite-volume central scheme [4].

The operating and design parameters used to generate the blade geometries are shown in Tabs. 4, 5 for nozzle guide vane and rotor, respectively, the working fluid being R245fa. As shown in Fig. 10, the nominal working conditions for stator and rotor are chosen in order to expand the organic fluid in the dense gas region and maximise the dense gas effects.

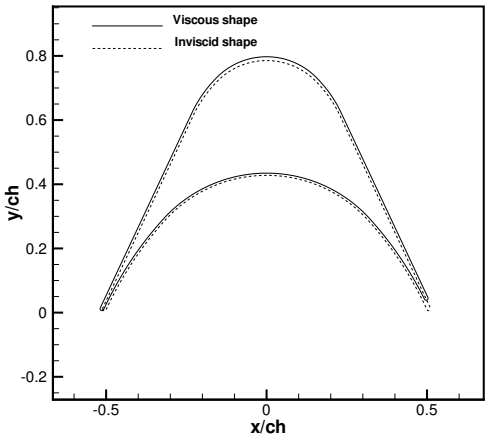

FIGURE 9 – Comparison between inviscid and viscous impulse rotor blade shapes.

TABLE 4 – Operating and design parameters for the nozzle guide vane design.

p_r^0	T_r^0	$\beta[p_0/p_{out}]$	M_{out}	$G[kg/s]$	Θ_f [◦]
0.9	1.05	3.3	1.5	0.458	70.0

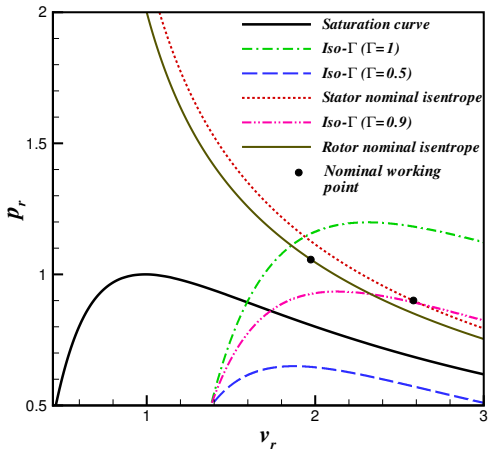

FIGURE 10 – Clapeyron diagram of the Peng-Robinson-Stryjek-Vera saturation curve, iso-Γ lines and nominal isentropes for stator and rotor. The working fluid is R245fa.

4.1 Isolated stator

For an expander with a low degree of reaction, the main part of the expansion is carried out in the nozzle guide vanes. The accuracy of the MOC design and the main nozzle guide vane performances have been assessed by means of a viscous simulation. The operating and design parameters are listed in Tab. 4.

The target exit Mach number is set to 1.5 with an expansion pressure ratio $\beta = p_0/p_{out} = 3.3$. The calculations are carried out on a C-type grid with $384 \cdot 128$ cells, chosen after a suitable

TABLE 5 – Operating and design parameters for the rotor design.

p_r^0	T_r^0	M_{in}	M_{out}	M_l	M_u	β_{in}	β_{out}
1.05	1.05	1.7	1.7	1.1	1.9	60°	60°

TABLE 6 – Summary of the guide vane performances for R245fa fluid, viscous calculations and blade shape calculated by means of the REF model, with and without boundary layer correction.

BL corr.	η_{is}	Θ_C	Power out. [kW]	G [kg/s]
No	0.886	0.135	1.640	0.447
Yes	0.912	0.182	1.697	0.452

convergence study. As a general remark, we observe that in viscous calculations the isentropic efficiency drops by about 10% with respect to the inviscid value. Besides, the pressure expansion ratio is affected by the reduction of the effective exit-to-throat area ratio with consequences on the exit Mach number and power output. These effects are due to the viscous losses in the attached boundary layer and in the wake, as well as to the formation of a separation bubble at the suction side, close to trailing edge, leading to a significant reduction of the effective exit-to-throat area ratio. These undesirable phenomena are mitigated when applying the boundary layer correction to the blade design. The results in terms of Mach number contours are shown in Fig. 11. It can be noticed that the Mach number at the trailing edge (pressure side) is respectful of the target value $M_e = 1.5$. Besides, the pressure distribution (pressure side) in the divergent (and thus the pressure ratio) is much closer to the target inviscid one with respect than in the case of a design without boundary layer correction (see Fig. 12). A strong supersonic expansion is observed at the blade trailing edge, due to the strong deflection of the supersonic flow. As a result, an average Mach number of about 2 is obtained at the stator outlet

In the divergent part of the nozzle, the absence of normal shocks shows that the adapted nozzle design realizes the actual pressure distribution, at the given total conditions. On the trailing-edge oblique shock is also present in the viscous simulation, but it is weaker than in the inviscid case. As a consequence, the increased losses are essentially due to the viscous phenomena. The main nozzle performance parameters are shown in Tab. 6, in terms of isentropic efficiency η_{is}, Carnot factor $\Theta_C = 1 - T_0/T$, defined as the Carnot efficiency of a thermal machine operating between the total temperature T_0 and the local static temperature T, power output and massflow rate. The results are compared with those obtained without boundary layer correction. It can be noticed an increase of all the parameters, especially the isentropic efficiency is improved of 2.8%, thanks to the reduction of the viscous effects due to the viscous wake. The Carnot factor increases by 25%, showing that the heat source is better exploited. The power output is improved too, with an increase of 3.3%, due to the more accurate approximation of the target pressure distribution and the 1.1% higher massflow rate, which is closer to the design value $G = 0.458$ kg/s.

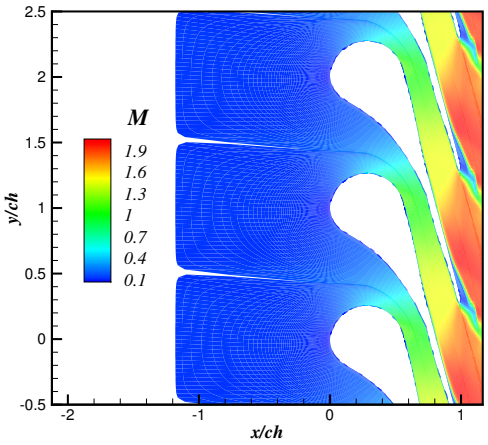

FIGURE 11 – Mach number contour plot for the nozzle guide vane (viscous simulation with R245fa fluid).

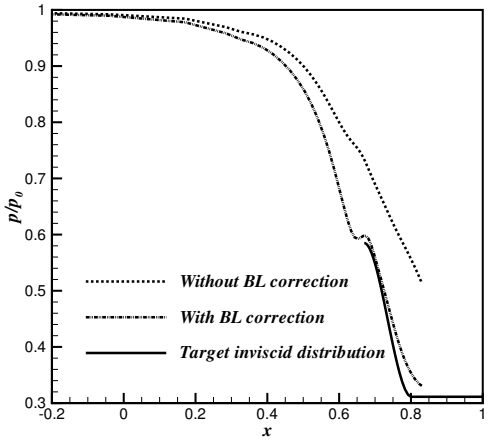

FIGURE 12 – Nozzle guide vane axis pressure distribution with and without boundary layer correction, and comparison with the target inviscid distribution.

4.2 Isolated rotor

A viscous calculation has been carried out for the isolated rotor designed with the MOC in order to verify the accuracy of the design methodology. The periodicity problem due to the unique incidence has been taken into account by means of the approach shown in the preceding section, which was used to calculate the appropriate inlet relative flow angle.

Tab. 5 provides the main parameters used for the design of the rotor cascade. The thermodynamic conditions are slightly supercritical in order to work in a highly non-ideal thermodynamic region and the working fluid is R245fa. The isolated rotor flow domain has been split into 9 structured blocks by using H-shaped blocks at the inlet and outlet of the domain and one O-shaped block around the blade for the clustering of cells on the wall, in order to take into account the development of the boundary layer. A non-reflecting inlet, pressure-outlet, periodic and adiabatic wall boundary conditions have been imposed. The overall number of mesh cells

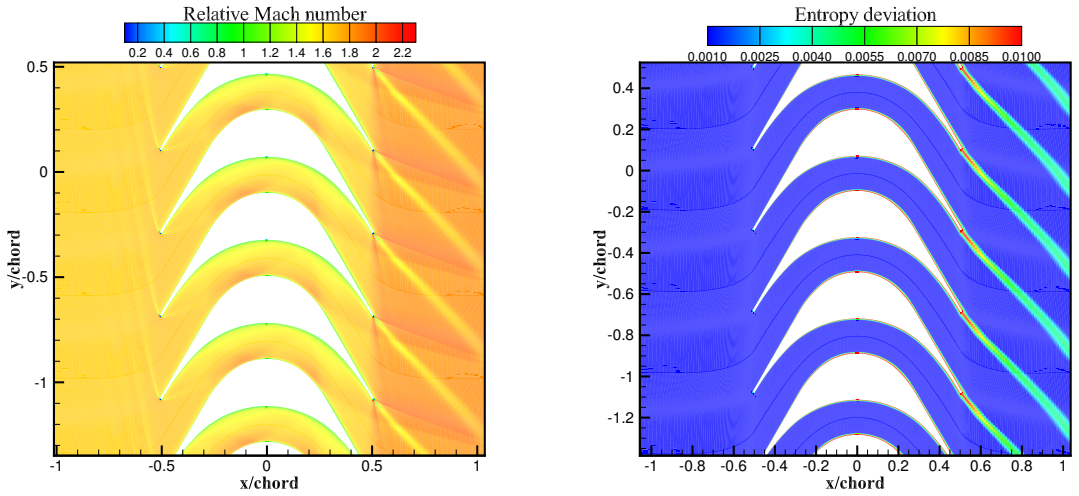

(a) (b)

FIGURE 13 – Mach number contour (a) and entropy deviation (b) for DGMOC blades (no boundary layer correction).

is 196604 cells) and the height of the first cell close to the wall has been set equal to $1 \cdot 10^{-6}$ times the axial chord, leading to $y^+ \approx 1$. The results are shown in Figs. 13 in terms of relative Mach number and entropy deviation, the latter being defined as the relative entropy variation $(s - s_{in})/s_{in})$ with respect to the inlet entropy s_{in}. The figure shows that the DGMOC design provides a started rotor with a bow-shock on the leading edges that confirms the presence of the unique incidence problem. Inside the rotor vane, the flow pattern is characterized by successive reflections of the bow-shock. Two oblique shocks depart from the trailing edge and interact with the viscous wake. The boundary layer development modifies the effective flow passage area and affects the performance of the cascade, which can be evaluated in terms of degree of reaction Λ and entropy deviation. The calculation of Λ is based on the average static enthalpies at the rotor inlet and outlet, $\Lambda = \frac{\Delta h_{rotor}}{\Delta h_{total}}$. Since the rotor is isolated, a reference constant value has been assigned to Δh_{total} in order to calculate Λ. The DGMOC design without boundary layer correction provides $\Lambda = -0.034$, which is slightly different the nominal value (zero degree of reaction). The negative value implies that the supersonic flow undergoes a compression, leading to a non symmetric effective area distribution.

The analysis of the entropy deviation, reported in Figs. 13b shows that the losses are localised in the turbulent boundary layer and around the trailing edge. Afterwards, a CFD simulation has been carried out for the rotor modified by the boundary layer correction and the results have been compared to those previously obtained for a purely inviscid design. The Mach number and entropy deviation distributions for the corrected rotor are reported in Fig. 14. The Mach number shows a similar shock pattern with several reflections through the blade vane up to the exit. The rotor is again fully started. The corrected design leads to lower losses, in terms of entropy deviation, since the boundary layer remains thinner (no spurious compression in this case), and so does the wake (Fig. 14b). The boundary layer correction has a beneficial effect also on the degree of reaction ($\Lambda = -0.011$), which remains closer to zero than in the preceding case. Fig. 15) diplays the pressure distribution along the blade wall. The numerical results for the DGMOC geometries with and without boundary layer corrections are compared

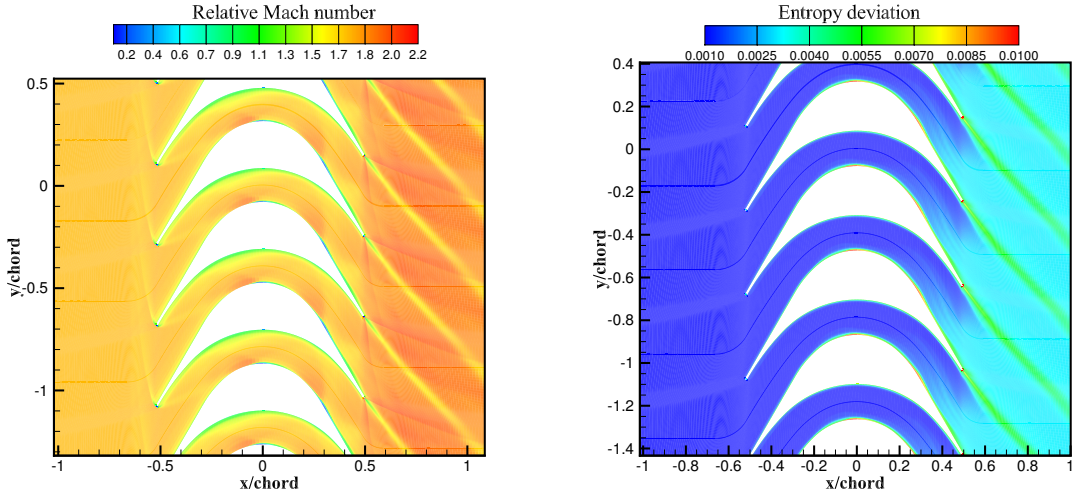

(a) (b)

FIGURE 14 – Mach number contour plot (a) and entropy deviation (b) for RODEC rotors with boundary layer correction.

with the target design distribution corresponding to the inviscid DGMOC solution, as well as with the solution obtained for a simple circular arc design. The corrected DGMOC solution is in rather fair agreement with the nominal one, except for some residual oscillations on the pressure and suction sides due to reflections of the (weak) bow shock, which are not present in the nominal design (corresponding to zero leading edge thickness).

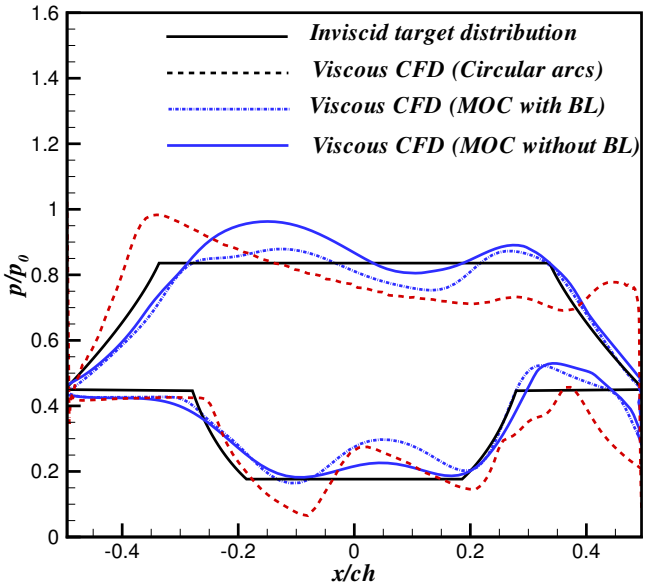

FIGURE 15 – Wall pressure distribution on the rotor blade for the viscous simulation with boundary layer correction and comparison with the target design distribution.

5 Conclusions

A fast design methodology of supersonic turbines for ORC applications based on an extended method of characteristics (DGMOC) has been developed. Dense gas effects are accurately taken into account in the preliminary design stage by means of advanced EOS. Rotor design is supplemented by an investigation of the unique incidence problem in the dense gas regime, for which a numerical approach is developed. A further improvement in the design approach of both stator and rotor has been carried out by correcting the "inviscid" shape provided by the DGMOC by means of the boundary layer thickness, computed by solving the compressible boundary layer equations along with dense gas models for the thermodynamic properties.

Numerical simulations have been carried out to assess the performance of the nozzle guide vane, showing that the isentropic efficiency and the power output improve by approaching the design target values when the boundary layer correction is performed.

The supersonic rotor design has been also verified by means of viscous numerical simulations. The solution of the unique incidence problem in dense gas regime allows to prescribe the inlet flow angle allowing to achieve the nominal Mach number at the rotor leading edge (downstream of the bow shock). As a consequence the numerical results can be compared with the target design distributions for the ideal, unshocked case. Using boundary layer corrections ensures a fairer agreement between the numerically computed and the target pressure wall distribution and degree of reaction, thanks to the mitigation of re-compression effect due to the reduction of the effective blade passage.

Références

[1] A. C. Aldo and B. M. Argrow. Supersonic minimum length nozzle design for dense gases. *Journal of Fluids Engineering*, 17 :270–276, 1993.

[2] L. Budugur. *Fluid Dynamics and Heat Transfer of Turbomachinery.* Wiley-Interscience, 1995.

[3] E. Bufi. *Robust optimization of ORC turbine expanders.* PhD thesis, ENSAM, 2016.

[4] P. Cinnella and P. M. Congedo. Numerical solver for dense gas flows. *AIAA journal*, 43(11) :2458–2461, 2005.

[5] M. Cramer and A. Crickenberger. Prandtl-meyer function for dense gases. *AIAA journal*, 30(2) :561–564, 1992.

[6] F. E. Culick. A turbulent analog of the stewartson-illingworth transformation. *Journal of the Aerospace Sciences*, 2012.

[7] J. Délery. *Handbook of compressible aerodynamics.* ISTE, 2010.

[8] E. Eckert. Engineering relations for friction and heat transfer to surfaces in high velocity flow, 1955.

[9] L. J. Goldman. Analytical investigation of supersonic turbomachinery blading. 1/2-analysis of impulse turbine-blade sections. *NASA -TN D-4421*, 1968.

[10] A. Guardone, A. Spinelli, and V. Dossena. Influence of molecular complexity on nozzle design for an organic vapor wind tunnel. *Journal of Engineering for Gas Turbines and Power*, 135(4) :042307, 2013.

[11] E. W. Lemmon, M. L. Huber, and M. O. McLinden. *NIST Reference Fluid Thermodynamic and Transport Properties - REFPROP Version 9.1.* NIST, 2013.

[12] E. W. Lemmon and R. Span. Short fundamental equations of state for 20 industrial fluids. *Journal of Chemical & Engineering Data*, 51(3) :785–850, 2006.

[13] E. Maskell. Approximate calculation of the turbulent boundary layer in two-dimensional incompressible flow. *Royal Aircraft Est., Farnborough, Gt. Britain, Report Aero*, 2443, 1951.

[14] W. Moeckel. Approximate method for predicting form and location of detached shock waves ahead of plane or axially symmetric bodies. *NACA-TN-1921*, 1949.

[15] G. Paniagua, M. Iorio, N. Vinha, and J. Sousa. Design and analysis of pioneering high supersonic axial turbines. *International Journal of Mechanical Sciences*, 89 :65–77, 2014.

[16] E. Reshotko and M. Tucker. Approximate calculation of the compressible turbulent boundary layer with heat transfer and arbitrary pressure gradient. *NASA-TN-4154*, 1957.

[17] L. Sciacovelli and P. Cinnella. Numerical investigation of dense gas flows through transcritical multistage axial organic rankine cycle turbines. *Journal for gas turbines and power*, 2013.

[18] H. Starken, Z. Yongxing, and H.-A. Schreiber. Mass flow limitation of supersonic blade rows due to leading edge blockage. In *ASME 1984 International Gas Turbine Conference and Exhibit*, pages V001T01A064–V001T01A064. American Society of Mechanical Engineers, 1984.

[19] R. Stryjek and J. Vera. Prsv : An improved peng–robinson equation of state for pure compounds and mixtures. *The canadian journal of chemical engineering*, 64(2) :323–333, 1986.

[20] P. A. Thompson. A fundamental derivative in gasdynamics. *Physics of Fluids (1958-1988)*, 14(9) :1843–1849, 1971.

[21] A. P. Wheeler and J. Ong. The role of dense gas dynamics on orc turbine performance. In *ASME Turbo Expo 2013 : Turbine Technical Conference and Exposition*, page V002T07A030. American Society of Mechanical Engineers, 2013.

[22] M. J. Zucrow and J. D. Hoffman. Gas dynamics. *New York : Wiley, 1976*, 1–2, 1976.